ChemistryOpen

Research Article
doi.org/10.1002/open.202100288

Chemistry Europe
European Chemical Societies Publishing

www.chemistryopen.org

MIL-100(Fe) Supported Pt–Co Nanoparticles as Active and Selective Heterogeneous Catalysts for Hydrogenation of 1,3-Butadiene

Lili Liu,* Zhixuan Han, Yifan Lv, Chunling Xin, Xiaojing Zhou, Lei Yu, and Xishi Tai*[a]

Superior catalytic performance for selective 1,3-butadiene (1,3-BD) hydrogenation can usually be achieved with supported bimetallic catalysts. In this work, Pt–Co nanoparticles and Pt nanoparticles supported on metal–organic framework MIL-100(Fe) catalysts (MIL=Materials of Institut Lavoisier, PtCo/MIL-100(Fe) and Pt/MIL-100(Fe)) were synthesized via a simple impregnation reduction method, and their catalytic performance was investigated for the hydrogenation of 1,3-BD. Pt1Co1/MIL-100(Fe) presented better catalytic performance than Pt/MIL-100(Fe), with significantly enhanced total butene selectivity. Moreover, the secondary hydrogenation of butenes was effectively inhibited after doping with Co. The Pt1Co1/MIL-100(Fe) catalyst displayed good stability in the 1,3-BD hydrogenation reaction. No significant catalyst deactivation was observed during 9 h of hydrogenation, but its catalytic activity gradually reduces for the next 17 h. Carbon deposition on Pt1Co1/MIL-100(Fe) is the reason for its deactivation in 1,3-BD hydrogenation reaction. The spent Pt1Co1/MIL-100(Fe) catalyst could be regenerated at 200 °C, and regenerated catalysts displayed the similar 1,3-BD conversion and butene selectivity with fresh catalysts. Moreover, the rate-determining step of this reaction was hydrogen dissociation. The outstanding activity and total butene selectivity of the Pt1Co1/MIL-100(Fe) catalyst illustrate that Pt–Co bimetallic catalysts are an ideal alternative for replacing mono-noble-metal-based catalysts in selective 1,3-BD hydrogenation reactions.

Introduction

Platinum (Pt) is an important transition metal and catalyst candidate due to its outstanding catalytic properties in chemical reactions.[1] In particular, Pt-based catalysts have been widely used in hydrogenation reactions with compounds such as 1,3-butadiene (1,3-BD),[2] CO_2,[3] cinnamaldehyde,[4] nitrobenzene,[5] aromatic heterocyclic compounds and carboxyl substituted aromatics,[6] tertiary amines,[7] and 5-hydroxymethylfurfural.[8] The selective hydrogenation of 1,3-BD is a significant industrial refining process that purifies butenes produced from crude oil cracking.[9] 1,3-BD can be selectively hydrogenated to butenes (such as 1-butene, trans-2-butene, and cis-2-butene), which improves carbon utilization.[10] However, these butenes can easily be further hydrogenated to butane due to the low barrier to this reaction.[11] Hence, improving butene selectivity is one of the most crucial factors for developing 1,3-BD hydrogenation catalysts. Currently, one of the most widely utilized approaches for increasing butene selectivity is the addition of a second metal element to single-metal materials to produce bimetallic catalysts.[9,10] This second metal can influence the surface structure and electronic properties of the metals, enhance the hydrogen adsorption ability of the catalyst, and decrease butene adsorption.[9] Therefore, catalyst activity and butene selectivity can be enhanced. Wang et al.[12] synthesized Pt–Ni/γ-Al_2O_3 and Pt–Ni/TiO_2 bimetallic catalysts that presented higher activities for 1,3-BD hydrogenation than corresponding single-metal catalysts. Lonergan et al.[13] also reported that Pt–Ni bimetallic catalysts exhibit significantly higher catalytic activity than monometallic Pt or Ni catalysts for the hydrogenation of 1,3-BD. Compared to a monometallic Pt/UiO-67 catalyst, a Au–Pt bimetallic AuPt/UiO-67-3 catalyst exhibited enhanced butene selectivity.[14] A Pt–Co/γ-Al_2O_3 catalyst demonstrated better activity than a monometallic Pt/γ-Al_2O_3 catalyst.[15] These prior results show that Pt-based bimetallic catalysts can act as high-efficiency 1,3-BD hydrogenation catalysts, demonstrating outstanding catalytic activity and selectivity for butenes.

Metal-organic frameworks (MOFs) are novel micro-mesoporous materials formed by the combination of transition metal ions or clusters with multidentate organic ligands.[16] Compared with carbon and metal oxide-based materials, MOFs display many positive characteristics, such as their low density, large BET surface area, high adsorption capacity, uniform pore distribution, and excellent chemical stability.[17] Therefore, MOFs are more conducive for the dispersion and stabilization of metal nanoparticles (NPs), and they display significant promise as supports for metal NPs.[17b,18] MIL-100(Fe) (MIL=Materials of Institut Lavoisier, $Fe^{III}_3O(H_2O)_2(F/OH)[C_6H_3(CO_2)_3]_2 \cdot 14.5H_2O$) is a prototypical example MOF with a rigid zeolitic architecture,

[a] Prof. L. Liu, Z. Han, Y. Lv, Prof. C. Xin, Prof. X. Zhou, Dr. L. Yu, Prof. X. Tai
School of Chemistry & Chemical Engineering and Environmental Engineering, Weifang University
Weifang, 261061, Shandong (P.R. China)
E-mail: liulili122@wfu.edu.cn
taixs@wfu.edu.cn

ChemistryOpen

Research Article
doi.org/10.1002/open.202100288

Chemistry
Europe
European Chemical
Societies Publishing

hierarchical pore texture, superior chemical and hydrolytic stability, and extremely high porosity. Thus, MIL-100(Fe) is an excellent catalyst support for heterogeneous catalysis.[19] Jing et al.[20] successfully synthesized a Ag/MIL-100(Fe) catalyst using a MIL-100(Fe) MOF as a support via a simple solution-based impregnation-reduction strategy. They reported that this Ag/ MIL-100(Fe) catalyst demonstrated excellent catalytic activity for the terminal alkyne photothermal carboxylation with CO_2. In this reaction system, different aromatic alkynes were transformed to their corresponding carboxylic acid products with yields of 86–92% after 12 h visible light irradiation under CO_2 (1 atm) at room temperature.[20] The Ag/MIL-100(Fe) catalyst also presented excellent recyclability performance, with its catalytic activity remaining almost constant after three cycles.[20] MIL-100(Fe) supported Pd–Ni alloy NPs (Pd–Ni@MIL-100(Fe)) displayed prominent catalytic performance for the reversible hydrogenation/hydrogenation of N-heterocycle derivatives.[21] The Pd–Ni@MIL-100(Fe) catalyst exhibited superior catalytic stability and no significant loss in activity after being reused six times.[21] Moreover, no distinct agglomeration was visible in TEM micrographs of the recycled catalyst due to the highly porous structure and superior stability in water of the MIL-100(Fe) support.[21]

In this study, the catalytic properties of PtCo/MIL-100(Fe) and Pt/MIL-100(Fe) were compared for the hydrogenation of 1,3-BD. The effect of the Pt:Co molar ratio on catalytic performance as well as the stability and reaction order of 1,3-BD hydrogenation over Pt1Co1/MIL-100(Fe) with respect to the reactant were also studied. This comparative study demonstrated that the bimetallic Pt1Co1/MIL-100(Fe) catalyst presented better catalytic properties than Pt/MIL-100(Fe), and the best 1,3-BD hydrogenation performance was achieved with a Pt:Co molar ratio of 1:1. No obvious catalytic activity deactivation or reduction in the selectivity to total produced butenes was observed during 9 h of reaction time on stream. The reaction order demonstrated that the rate-determining step of this hydrogenation reaction with Pt1Co1/MIL-100(Fe) is hydrogen dissociation.

Results and Discussion

As-prepared Catalyst Characterization

MIL-100(Fe), Pt/MIL-100(Fe), and Pt1Co1/MIL-100(Fe) were characterized using XRD, XPS, H_2-TPR, TEM, EDS, and nitrogen physisorption experiments. Compared to the XRD patterns of a typical sample of MIL-100(Fe), the MIL-100(Fe) synthesized herein is not crystalline and embedded with defects.[22] The XRD patterns of the Pt/MIL-100(Fe) and Pt1Co1/MIL-100(Fe) materials display the characteristic peaks of MIL-100(Fe), but these characteristic peaks decrease in intensity or entirely disappear after loading the Pt NPs and Pt–Co NPs (Figure S1 in Supporting Information). This phenomenon indicates that the Pt NP and Pt–Co NP loading process is detrimental to the MIL-100(Fe) structure.[23]

XPS analysis was conducted on Pt/MIL-100(Fe) and Pt1Co1/ MIL-100(Fe) to investigate the relative valence states of the loaded Pt and Co (Figure S2). For Pt/MIL-100(Fe), the Pt^{2+} $4f_{7/2}$ peak exists at a binding energy value of 72.96 eV, and the Pt^{2+} $4f_{5/2}$ peak is located at a binding energy value of 75.80 eV.[24] The Pt^{2+} 4f binding energy peaks of Pt1Co1/MIL-100(Fe) (73.04 eV and 76.29 eV) show a slightly positive shift compared to the corresponding Pt/MIL-100(Fe) spectrum, which suggested that the electronic structure of Pt was affected by Co. That is, there are electronic interactions between Pt and Co.[25] The Co and Pt form alloy NPs.[26] This analysis agrees with that reported in other work.[26] The fitted Co 2p spectrum of Pt1Co1/ MIL-100(Fe) exhibits peaks at 782.0 eV (Co^{2+} $2p_{1/2}$) and 796.0 eV (Co^{2+} $2p_{3/2}$).[27] The peak at 780.7 eV is assigned to Co^{3+} $2p_{3/2}$.[28] Meanwhile, two satellite peaks at 786.19 eV and 802.21 eV are assigned to the shakeup peaks of Co $2p_{1/2}$ and Co $2p_{3/2}$.[27] Co is deeply oxidized to Co^{3+} in Pt1Co1/MIL-100(Fe) catalyst, which could be attributed to the influence of MIL-100(Fe) environment. And any coordination of MIL-100(Fe) with Co could lead to this positive shift.

H_2 temperature-programmed reduction (H_2-TPR) profiles of Pt1Co1/MIL-100(Fe) presented four main reduction peaks at 143.4 °C, 172.0 °C, 363.9 °C, and 422.6 °C (Figure S3). The reduction peak at 172.0 °C is assigned to the reduction of oxidized Pt species to metallic Pt^0.[29] The peaks at 143.4 °C and 363.9 °C are associated with the reduction of Co_3O_4 to CoO and CoO to Co^0, respectively.[30] The higher temperature peak (422.6 °C) is assigned to the decomposition of the MIL-100(Fe) support.[31] These results are agree with the conclusions obtained from the XPS analysis: the existence of PtO, Co_3O_4, and CoO in the Pt1Co1/MIL-100(Fe) catalyst.

TEM, high-angle annular dark-field scanning TEM (HAADF-STEM), and EDS were used to investigate the size and distribution of the Pt–Co NPs and Pt NPs on MIL-100(Fe). The TEM images, HAADF-TEM images, EDS elemental mappings, and Pt–Co particle size distribution of Pt1Co1/MIL-100(Fe) and Pt/ MIL-100(Fe) are presented in Figure 1 and Figure S4. As shown in the TEM and HAADF-STEM images, the Pt–Co NPs and Pt NPs in Pt1Co1/MIL-100(Fe) and Pt/MIL-100(Fe) are uniformly loaded on the MIL-100(Fe) support. The Pt1Co1/MIL-100(Fe) and Pt/ MIL-100(Fe) catalysts display similar particle sizes: 3.1 nm and 2.9 nm, respectively. The EDS elemental mapping of Pt1Co1/ MIL-100(Fe) shows a uniform Pt and Co elemental distribution, confirming the formation of the Pt–Co alloy NPs.

Figure S5 presents nitrogen physisorption isotherms and pore size distribution of the bare MIL-100(Fe) MOF, Pt1Co1/MIL-100(Fe), and Pt/MIL-100(Fe) at 77 K. All samples present type IV adsorption isotherms, indicating their mesoporous nature.[32] As shown in Table 1, MIL-100(Fe) displays a high BET surface area (1473 m^2/g), while the BET surface areas of Pt1Co1/MIL-100(Fe) and Pt/MIL-100(Fe) catalysts are dramatically reduced (919 m^2/g and 585 m^2/g, respectively). Similarly, the pore volume of MIL-100(Fe) is 0.93 cm^3/g, while the pore volumes of Pt1Co1/MIL-100(Fe) and Pt/MIL-100(Fe) are lower (0.76 cm^3/g and 0.77 cm^3/ g, respectively) (Table 1). This significant reduction in surface area and pore volume is potentially caused by the Pt–Co NPs and Pt NPs occupying and/or blocking the pores of MIL-
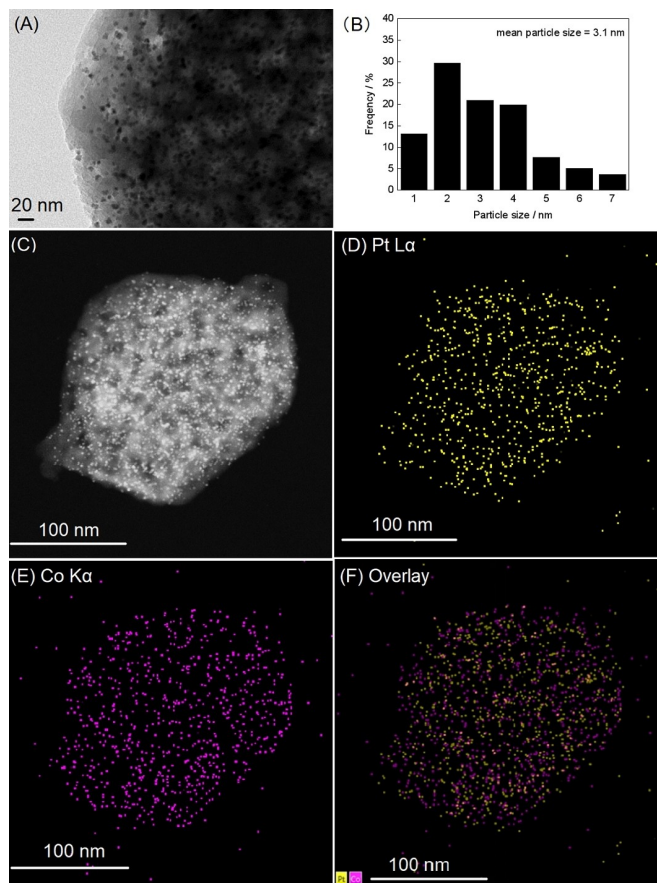
ChemistryOpen

Research Article
doi.org/10.1002/open.202100288

Chemistry
Europe
European Chemical
Societies Publishing

Figure 1. TEM image (A), Pt–Co particle size distribution (B), HAADF-TEM image (C), and EDS elemental mapping images of Pt1Co1/MIL-100(Fe) (D–F).

Table 1. The porous properties of MIL-100(Fe), Pt1Co1/MIL-100(Fe), and Pt/MIL-100(Fe)

samples	BET [m²/g]	volume [cm³/g]	mean pore diameter [nm]
MIL-100(Fe)	1473	0.93	2.5
Pt1Co1/MIL-100(Fe)	919	0.76	3.3
Pt/MIL-100(Fe)	585	0.77	5.3

100(Fe).[33] The mean pore diameter of MIL-100(Fe), Pt1Co1/MIL-100(Fe), and Pt/MIL-100(Fe) are 2.5, 3.3, and 5.3 nm, respectively. The mean pore diameter of MIL-100(Fe) increases markedly after loading the Pt–Co NPs and Pt NPs. This phenomenon may be due to the fact that the support of MIL-100(Fe) was not crystalline to begin with (going by the PXRD) and owing to defects and the subsequent loading of Pt–Co or Pt NPs, the pores of MIL-100(Fe) experienced further expansion. The pore size distribution curves of MIL-100(Fe), Pt1Co1/MIL-100(Fe), and Pt/MIL-100(Fe) display that the samples have both micropores and mesopores. The pore size distributions of MIL-100(Fe) and Pt1Co1/MIL-100(Fe) are mainly centered at 0.56, 1.25, and 3.76 nm. However, the monometallic Pt/MIL-100(Fe) presents different pore size distribution, and the pore size distribution is mainly centered at 0.56, 3.76, and 5.40 nm.

Catalyst Test

The Pt1Co1/MIL-100(Fe) and Pt/MIL-100(Fe) catalysts were evaluated for selective 1,3-BD hydrogenation at 70 °C under atmospheric pressure. Figure 2 shows 1,3-BD conversion and product selectivity as a functions of reaction time over the MIL-100(Fe), Pt1Co1/MIL-100(Fe), and Pt/MIL-100(Fe) at 70 °C. The MIL-100(Fe) catalyst is almost completely inactive for 1,3-BD hydrogenation under the employed conditions due to its lack of catalytic active sites. In contrast, the Pt1Co1/MIL-100(Fe) and Pt/MIL-100(Fe) catalysts display outstanding catalytic activity,
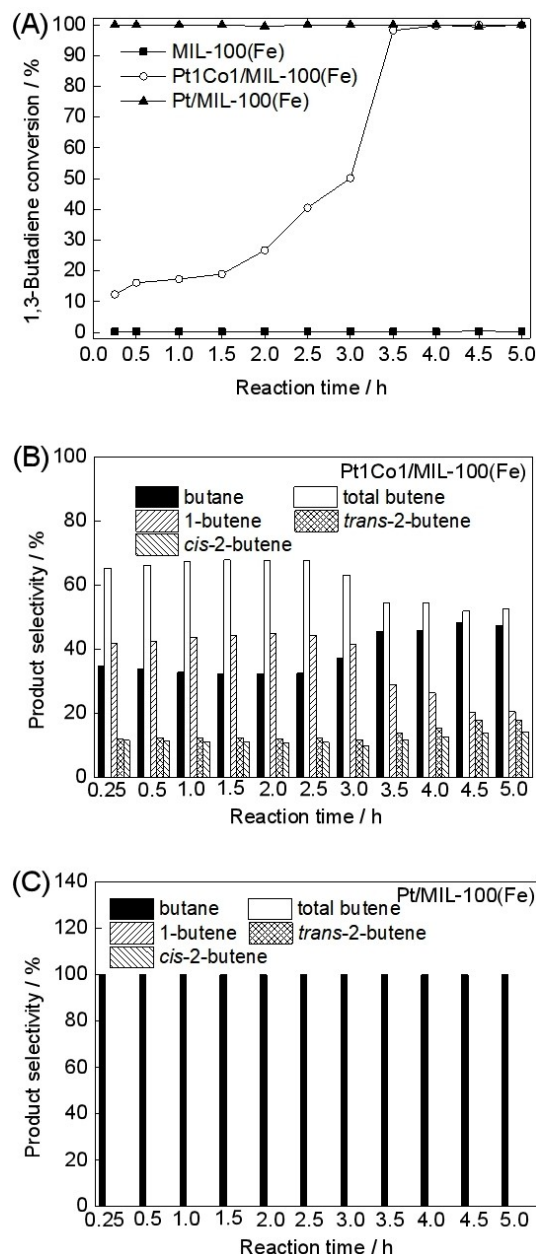

Figure 2. The conversion of 1,3-BD (A) and product selectivities (B, C) as functions of reaction time for 1,3-BD hydrogenation over the MIL-100(Fe), Pt1Co1/MIL-100(Fe), and Pt/MIL-100(Fe) catalysts (reaction conditions: 15 mg catalyst; 70 °C reaction temperature; 20 mL/min 1.0 vol% 1,3-BD/99.0 vol% N₂, 8.5 mL/min 99.999% H₂).

ChemistryOpen

Research Article
doi.org/10.1002/open.202100288

Chemistry
Europe
European Chemical
Societies Publishing

indicating that the Pt–Co NPs and Pt NPs can efficiently catalyze 1,3-BD hydrogenation. Using the Pt1Co1/MIL-100(Fe) catalyst, the conversion level of 1,3-BD increases with reaction time with an S-shaped growth curve. The conversion of 1,3-BD reaches 98.2% at 70 °C within 3.5 h and levels off as the reaction proceeds further. However, Pt/MIL-100(Fe) presents a differently shaped conversion curve. For this catalyst, the 1,3-BD conversion level is approximately 100% at all reaction times. Using the Pt1Co1/MIL-100(Fe) catalyst, the selectivities for formation butenes (1-butene, *trans*-2-butene, and *cis*-2-butene) slightly increase during the first 1.0 h of the reaction, with values ranging from 65.2% to 67.2%. These values remain essentially constant from 1.0 h to 2.5 h. From 3.0 h to 5.0 h, the selectivity to total butenes significantly decreases when the concentration of 1,3-BD rapidly drops. The total butene selectivity remains at about 54.0% when 1,3-BD is almost completely transformed. The selectivities to the various butene isomers with the Pt1Co1/MIL-100(Fe) catalyst show a similar distribution across the whole reaction time range. The various butene isomers are synthesized in the order 1-butene > *trans*-2-butene > *cis*-2-butene. Furthermore, Pt1Co1/MIL-100(Fe) demonstrates a clear reduction in the selectivity to 1-butene when the time on stream is higher than 3.0 h and 1,3-BD conversion is higher than 50.0%. In contrast, the selectivities of Pt1Co/MIL-100(Fe) to *trans*- and *cis*-2-butene increase as the reaction time increases beyond 3.0 h. However, the Pt/MIL-100(Fe) catalyst demonstrates 100% butane selectivity at all reaction time intervals. Therefore, under the tested catalytic reaction conditions, the Pt/MIL-100(Fe) catalyst promotes the secondary hydrogenation of butenes to butane. As a slightly lower 65 °C reaction temperature, the Pt/MIL-100(Fe) selectivity to total produced butenes increases to 59.9% (Figure S6B). However, the 1,3-BD conversion on Pt/MIL-100(Fe) decreases from 100% (at 70 °C) to 33.2% (at 65 °C) (Figure S6A). Compared with Pt/MIL-100(Fe), the total butene selectivity of Pt1Co1/MIL-100(Fe) for 1,3-BD hydrogenation is significantly enhanced. This indicates that secondary butene hydrogenation to butane is effectively inhibited by Co doping.

According to previously reported studies, the molar ratio of the metals in bimetallic catalysts can significantly affect their activity and selectivity.[9,14,34] Thus, the influence of the Pt:Co molar ratio on 1,3-BD hydrogenation over the PtCo/MIL-100(Fe) catalyst was investigated at 70 °C, as shown in Figure 3. A Pt:Co molar ratio of 1:1 results in the best 1,3-BD hydrogenation performance, with a 1,3-BD conversion of up to 99.7% (Figure 3A) and a selectivity to total produced butenes of 54.4% (Figure 3B). However, the Pt1Co3/MIL-100(Fe) catalyst (with a Pt:Co molar ratio of 1:3) exhibits low 1,3-BD conversion, with a conversion of only 36.8% within 5.0 h at 70 °C. The PtCo/MIL-100(Fe) catalysts with Pt:Co molar ratios of 1:2, 2:1, and 3:1 all exhibit 1,3-BD conversions of up to 100% within 0.5 h at 70 °C, but their selectivities to total produced butenes sharply decrease. For instance, total butene selectivity of the Pt3Co1/MIL-100(Fe) catalyst is only 18.4%. 1,3-BD is completely converted to butane on the Pt1Co2/MIL-100(Fe) and Pt2Co1/MIL-100(Fe) catalysts under these catalytic reaction conditions.

The stability of the Pt1Co1/MIL-100(Fe) catalyst for 1,3-BD hydrogenation at 70 °C was tested, as shown in Figure 4. The
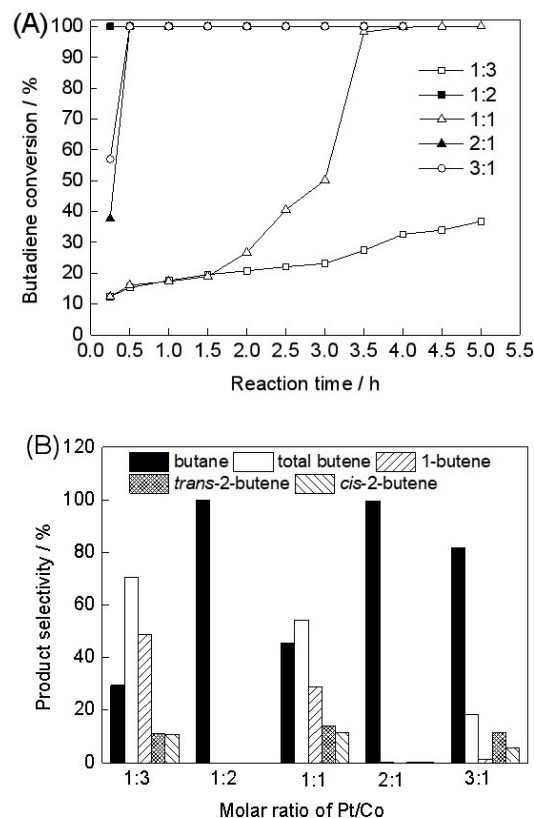

Figure 3. The effect of varying the Pt:Co molar ratio of PtCo/MIL-100(Fe) on (A) 1,3-BD conversion and (B) product selectivity (reaction conditions: 15 mg catalyst; 70 °C reaction temperature; 20 mL/min 1.0 vol% 1,3-BD/99.0 vol% N_2, 8.5 mL/min 99.999% H_2).
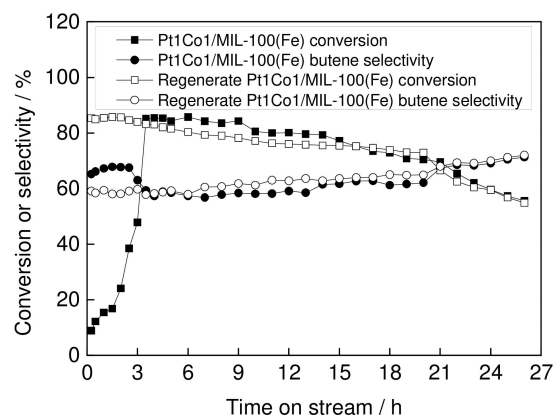

Figure 4. 26 h stability test of fresh Pt1Co1/MIL-100(Fe) and regenerate Pt1Co1/MIL-100(Fe) catalysts for 1,3-BD hydrogenation (reaction conditions: 10 mg catalyst; 70 °C reaction temperature; 20 mL/min 1.0 vol% 1,3-BD/ 99.0 vol% N_2, 8.5 mL/min 99.999% H_2).

Pt1Co1/MIL-100(Fe) catalyst does not exhibit any deactivation in the first 9 h, but its catalytic activity gradually reduces over the next 17 h. The catalyst displays 1,3-BD conversion of about 85% for the first 9 h, and this declines to 55.6% at 26 h. The selectivity to total produced butenes does not significantly change in the first 13 h, and then gradually increased over next 13 h. Carbon will be deposited on the catalysts during the 1,3-

ChemistryOpen

Research Article
doi.org/10.1002/open.202100288

**Chemistry
Europe**

European Chemical
Societies Publishing

BD hydrogenation process as films which will block the surface of active sites and inhibit the catalytic reaction.[35] The spent Pt1Co1/MIL-100(Fe) was regenerated at 200 °C in a flow of 12 mL/min N_2. The regenerated Pt1Co1/MIL-100(Fe) catalyst displayed the similar 1,3-BD conversion and total butene selectivity with fresh catalysts, indicating that Pt1Co1/MIL-100(Fe) could be regenerate at 200 °C and carbon deposition on Pt1Co1/MIL-100(Fe) is the reason for its deactivation in 1,3-BD hydrogenation reaction (Figure 4). The stability test for the Pt1Co3/MIL-100(Fe) was also carried out (Figure S7). Pt1Co3/MIL-100(Fe) displayed similar deactivation trend with Pt1Co1/MIL-100(Fe). In addition, an XRD pattern of the used Pt1Co1/MIL-100(Fe) catalyst after the 26 h reaction is not significantly different than that of the fresh catalyst (Figure S8). The TEM characterization was carried out on the spent Pt1Co1/MIL-100(Fe) after 26 h of reaction (Figure S9). The Pt–Co NPs in spent Pt1Co1/MIL-100(Fe) are uniformly dispersed on the MIL-100(Fe) support, and mean Pt–Co NP size is 3.1 nm. The spent Pt1Co1/MIL-100(Fe) and fresh Pt1Co1/MIL-100(Fe) catalysts showed the same mean Pt–Co NP size, indicating that no agglomeration of Pt–Co NPs occurred under the reaction conditions, which was probably attributed to the limitation effect of the MIL-100(Fe) channels.

In order to study the influence of the valence state of Pt and Co on 1,3-BD hydrogenation catalytic performance, the Pt1Co1/MIL-100(Fe)-200 catalyst was synthesized using the similar method as Pt1Co1/MIL-100(Fe), except reduced at 200 °C for 1 h under 10.0 mL/min H_2. XPS and H_2-TPR indicated that Pt and Co in Pt1Co1/MIL-100(Fe) are present in the mixture of PtO, Co_3O_4 and CoO, respectively. H_2-TPR of Pt1Co1/MIL-100(Fe) presented that Co^{3+} and Pt^{2+} could reduced to Co^{2+} and Pt^0 at 143.4 °C and 172.0 °C, respectively. Figure S10 shows 1,3-BD conversion and product selectivity as functions of reaction time on Pt1Co1/MIL-100(Fe)-200. Compared with Pt1Co1/MIL-100(Fe), Pt1Co1/MIL-100(Fe)-200 exhibits different catalytic performance in 1,3-BD hydrogenation reaction. The conversion of 1,3-BD gradually decreases with reaction time (Figure S10A). The 1,3-BD conversion was close to 100% within 15 min at 70 °C, while the conversion of 1,3-BD was only 18.7% after reaction 14 h. However, the selectivity to produced total butenes remains essentially constant at first 2.5 h (49.2%–49.7%), and then continuously increases with increasing reaction time (Figure S10B). The selectivity toward 1-butene and *cis*-2-butene increased gradually with increasing reaction time whilst that toward *trans*-2-butene decreased with increasing reaction time, indicating that some isomerizations occurred in the processing of reaction.[34] These results presented that Pt1Co1/MIL-100(Fe)-200 with Pt^0–CoO as active sites is more likely to deposit carbon during the reaction, and has poor stability for the 1,3-BD hydrogenation reaction.

The reaction order over the Pt1Co1/MIL-100(Fe) catalyst for 1,3-BD hydrogenation with respect to the reactants was obtained by varying the flow rate of one reactant while fixing the concentration of the other reactant at 70 °C. The 1.0 vol% 1,3-BD in N_2 flow rate was varied between 13.0 mL/min and 20 mL/min, while the hydrogen flow rate was varied between 4.5 mL/min and 10.5 mL/min. A log-log plot of the 1,3-BD consumption rate versus the 1,3-BD concentration at 70 °C provides a straight line with the equation: $\lg(-dC_{butadiene}/dt) = -0.63 \times \lg(C_{butadiene}) - 6.44$. For this equation, $R^2 = 0.99$, and the slope is equal to -0.63 (Figure S11A). A log-log plot of hydrogen consumption rate versus hydrogen concentration also provides a straight line: $\lg(-dC_{H2}/dt) = 0.72 \times \lg(C_{H2}) + 0.16$, where the slope is 0.72 and $R^2 = 0.99$ (Figure S11B). The apparent reaction orders of 1,3-BD hydrogenation with respect to 1,3-BD and hydrogen are -0.63 and 0.72, respectively. The negative reaction order of 1,3-BD (-0.63) shows that competitive adsorption exists between 1,3-BD and hydrogen on the pores and surface of Pt1Co1/MIL-100(Fe).[36] In other words, the existence of 1,3-BD potentially inhibits the hydrogenation of 1,3-BD.[36] The positive apparent reaction order with respect to hydrogen (0.72) indicates that a low amount of hydrogen is adsorbed on the pores and surface of Pt1Co1/MIL-100(Fe) and that the rate-limiting step of this reaction is hydrogen dissociation.[36a] These reaction orders differ from other previously reported values.[37] The reaction orders with respect to 1,3-BD and hydrogen are within the range of 0.40–0.66 and 0.31–0.73 reported for Pt/SiO_2 catalysts with different Pt particle sizes.[37] A Pt foil catalyst was reported to have reaction orders of -0.1 and 1.16 for 1,3-BD and hydrogen in 1,3-BD hydrogenation.[38]

Conclusion

In summary, 1,3-BD hydrogenation over PtCo/MIL-100(Fe) and Pt/MIL-100(Fe) catalysts was compared using a continuous flow fixed-bed microreactor. Compared with a monometallic Pt/MIL-100(Fe) catalyst, the bimetallic Pt–Co catalysts demonstrated significantly enhanced selectivity for 1,3-BD hydrogenation. The molar ratio of Pt:Co strongly influenced catalytic performance. The catalyst with the strongest catalytic performance, had a Pt:Co molar ratio of 1:1, and this catalyst demonstrated a high 1,3-BD conversion (99.7%) and total butene selectivity (54.4%) at 70 °C. The spent Pt1Co1/MIL-100(Fe) catalyst could be regenerated at 200 °C. Carbon deposition on Pt1Co1/MIL-100(Fe) is the reason for its deactivation in 1,3-BD hydrogenation reaction. The reaction orders of this system with respect to 1,3-BD and hydrogen were -0.63 and 0.72 for the Pt1Co1/MIL-100(Fe), indicating that hydrogen dissociation was the rate-limiting step. Overall, the results and analysis reported herein demonstrate that Pt–Co bimetallic catalysts are an ideal alternative for replacing mono-noble-metal-based catalysts in selective 1,3-BD hydrogenation reactions.

Experimental Section

MIL-100(Fe) Synthesis

A hydrothermal method was used to prepare MIL-100(Fe).[16a] Briefly, 5 mmol $Fe(NO_3)_3 \cdot 9H_2O$ and 3.35 mmol 1,3,5-benzenetricarboxylic acid were dissolved together in 25 mL deionized water while being stirred for 0.5 h at 500 rpm. Next, the resulting homogeneous solution was poured to a 100 mL Teflon-lined

ChemistryOpen

Research Article
doi.org/10.1002/open.202100288

**Chemistry
Europe**
European Chemical
Societies Publishing

autoclave reactor. The reaction was performed in the autoclave for 12 h at 150 °C. After the reaction, the resulting solid product was separated by centrifugation, and absolute ethanol was used to wash the solid at 90 °C for 12 h under stirring at 500 rpm. Finally, the washed solid was dried at 150 °C under 0.1 MPa vacuum.

Catalyst Synthesis

The PtCo/MIL-100(Fe) catalyst was prepared using an impregnation reduction method. First, $H_2PtCl_6 \cdot 6H_2O$ (26.7 mg) and Co-$(NO_3)_3 \cdot 6H_2O$ (15.0 mg) were dissolved in 1 mL absolute ethanol. Next, this solution was dropped on the MIL-100(Fe) support (0.2 g). This catalyst was dried at a temperature 50 °C for 2 h under a pressure of −0.1 MPa. The dried catalyst was then reduced for 1 h at 100 °C under H_2 (99.999% H_2, flowrate of 10.0 mL/min) to obtain Pt1Co1/MIL-100(Fe). Different Pt–Co bimetallic catalysts with varying molar ratios of Pt to Co were prepared using the same procedure. The theoretical Pt loading amount of the catalysts was fixed at about 5 wt%. The obtained bimetallic Pt–Co catalysts were denoted PtxCoy/MIL-100(Fe), with x:y molar ratios of 3:1, 2:1, 1:2, or 1:3. A Pt/MIL-100(Fe) (5 wt% Pt) catalyst was also synthesized using a similar impregnation reduction method. The catalyst Pt1Co1/MIL-100(Fe)-200 was also obtained using the similar method as Pt1Co1/MIL-100(Fe), except reduced at 200 °C for 1 h under 10.0 mL/min H_2. The actual Pt and Co content in the fresh Pt–Co and Pt catalysts was measured by ICP-OES. The Pt and Co levels in the Pt3Co1/MIL-100(Fe), Pt2Co1/MIL-100(Fe), Pt1Co1/MIL-100(Fe), Pt1Co2/MIL-100(Fe), and Pt1Co3/MIL-100(Fe) catalysts were 4.08 wt% and 0.45 wt%, 4.03 wt% and 0.67 wt%, 3.96 wt% and 1.26 wt%, 4.05 wt% and 2.71 wt%, and 3.91 wt% and 3.46 wt%, respectively. The actual content of Pt in Pt/MIL-100(Fe) was 4.41 wt%.

Catalytic Testing

The bimetallic Pt–Co and monometallic Pt catalysts were used to perform selective 1,3-BD hydrogenation under atmospheric pressure. The reactor was a continuous flow fixed-bed quartz tube microreactor (6 mm inner diameter). 10–15 mg catalyst powder and 500 mg quartz sand (25–50 mesh) were thoroughly mixed and packed into the quartz tube reactor. The temperature of the reactor was controlled by a tubular furnace (model #KSL-F, Tianjin Tongda Experimental Electric Furnace Factory) equipped with a temperature controller (model #TCW-3213, Tianjin Tongda Experimental Electric Furnace Factory). The inlet flowrate consisted of a 20 mL/min flow rate of 1 vol% 1,3-BD in 99 vol% N_2 and an 8.5 mL/min flow rate of 99.999% H_2. This mixed gas was flowed through the microreactor catalyst bed. The reaction products at the outlet were analyzed using an on-line gas chromatograph (SP-6890 instrument, Shandong Lunan Ruihong Chemical Instrument Co., Ltd.). The spent Pt1Co1/MIL-100(Fe) was regenerated at 200 °C in a flow of 12 mL/min N_2. The catalytic performance of regenerated Pt1Co1/MIL-100(Fe) catalyst in the 1,3-BD hydrogenation reaction was also studied under the same conditions as above.

Conflict of Interest

The authors declare no conflict of interest.

Data Availability Statement

Research data are not shared.

[1] a) K. J. Noh, H. Im, C. Lim, M. G. Jang, I. Nam, J. W. Han, *Chem. Eng. J.* **2022**, *427*, 131568–131576; b) J. Ye, B. Cheng, J. Yu, W. Ho, S. Wageh, A. A. Al-Ghamdi, *Chem. Eng. J.* **2022**, *430*, 132715–132723; c) H. L. Ye, S. X. Liu, C. Zhang, Y. Q. Cai, Y. F. Shi, *RSC Adv.* **2021**, *11*, 29287–29297; d) K. P. Reddy, H. Choi, D. Kim, M. Choi, R. Ryoo, J. Y. Park, *Chem. Commun.* **2021**, *57*, 7382–7285; e) J. T. Du, H. Niu, H. Wu, X. F. Zeng, J. X. Wang, J. F. Chen, *Int. J. Hydrogen Energy* **2021**, *46*, 25081–25091; f) K. Shafqat, S. Pitkäaho, M. Tiainen, L. Matějová, R. L. Keiski, *Nanomaterials* **2021**, *11*, 195–207.
[2] a) Y. Jiang, G. Liu, S. Wu, X. Zhang, X. Dai, Q. Sheng, Y. Wang, H. Wang, *Microporous Mesoporous Mater.* **2019**, *288*, 109557–109565; b) C. Hu, J. Sun, D. Wang, M. Peng, M. Shao, Q. Zhu, D. Ma, *ChemPhysChem* **2019**, *20*, 1804–1811.
[3] a) Z. Huang, Y. Yuan, M. Song, Z. Hao, J. Xiao, D. Cai, A. R. Ibrahim, G. Zhan, *Chem. Eng. Sci.* **2022**, *247*, 117106–117119; b) Y. Kuwahara, T. Mihogi, K. Hamahara, K. Kusu, H. Kobayashi, H. Yamashita, *Chem. Sci.* **2021**, *12*, 9902–9915; c) Y. Xie, J. Zuo, X. Liu, Y. Yang, F. Zhao, Y. Yuan, *Chinese Sci. Bull.* **2021**, *66*, 1144–1156.
[4] M. Stucchi, M. Manzoli, F. Bossola, A. Villa, L. Prati, *Nanomaterials* **2021**, *11*, 362–373.
[5] A. Prekob, G. Muránszky, M. Szőri, G. Karacs, F. Kristály, T. Ferenczi, B. Fiser, B. Viskolcz, L. Vanyorek, *Nanotechnology* **2021**, *32*, 425701–425712.
[6] M. Wang, M. Guo, X. Ren, X. Liu, Q. Yang, *J. Phys. Chem. C* **2021**, *125*, 15275–15282.
[7] G. J. Roeder, H. R. Kelly, G. Yang, T. J. Bauer, G. L. Haller, V. S. Batista, E. Baráth, *ACS Catal.* **2021**, *11*, 5405–5415.
[8] X. Wang, C. Zhang, B. Jin, X. Liang, Q. Wang, Z. Zhao, Q. Li, *Catal. Sci. Technol.* **2021**, *11*, 1298–1310.
[9] F. Lu, D. Sun, X. Jiang, *New J. Chem.* **2019**, *43*, 13891–13898.
[10] N. Hu, X. Y. Li, S. M. Liu, Z. Wang, X. K. He, Y. X. Hou, Y. X. Wang, Z. Deng, L. H. Chen, B. L. Su, *Chin. J. Catal.* **2020**, *41*, 1081–1090.
[11] a) B. Yang, X. Q. Gong, H. F. Wang, X. M. Cao, J. J. Rooney, P. Hu, *J. Am. Chem. Soc.* **2013**, *135*, 15244–15250; b) Z. Wang, D. Brouri, S. Casale, L. Delannoy, C. Louis, *J. Catal.* **2016**, *340*, 95–106.
[12] T. F. Wang, G. Mpourmpakis, W. W. Lonergan, D. G. Vlachos, J. G. G. Chen, *Phys. Chem. Chem. Phys.* **2013**, *15*, 12156–12164.
[13] W. W. Lonergan, D. G. Vlachos, J. G. Chen, *J. Catal.* **2010**, *271*, 239–250.
[14] L. Liu, X. Tai, X. Zhou, L. Liu, X. Zhang, L. Ding, Y. Zhang, *J. Taiwan Inst. Chem. Eng.* **2020**, *114*, 220–227.
[15] W. W. Lonergan, X. Xing, R. Zheng, S. Qi, B. Huang, J. G. Chen, *Catal. Today* **2011**, *160*, 61–69.
[16] a) D. Ozer, O. Icten, N. Altuntas-Oztas, B. Zumreoglu-Karan, *Res. Chem. Intermed.* **2020**, *46*, 909–922; b) Y. Han, Y. Zhang, Y. Zhang, A. Cheng, Y. Hu, Z. Wang, *Appl. Catal. A* **2018**, *564*, 183–189.
[17] a) W. He, Z. Li, S. Lv, M. Niu, W. Zhou, J. Li, R. Lu, H. Gao, C. Pan, S. Zhang, *Chem. Eng. J.* **2021**, *409*, 128274–128286; b) W. Sun, L. Luo, J. Li, X. Tian, D. Yan, Y. Zhu, *Catal. Lett.* **2022**, *152*, 570–584.
[18] Y. Xing, J. Li, M. Chen, X. Wang, X. Hou, *Microchim. Acta* **2021**, *188*, 225–233.
[19] a) J. N. Hall, P. Bollini, *ACS Catal.* **2020**, *10*, 3750–3763; b) N. A. Johari, N. Yusof, A. F. Ismail, *Mater. Today: Proc.* **2021**, *46*, 1954–1958.
[20] P. Jing, B. Wu, Z. Han, W. Shi, P. Cheng, *Chin. Chem. Lett.* **2021**, *32*, 3505–3508.
[21] J. W. Zhang, D. D. Li, G. P. Lu, T. Deng, C. Cai, *ChemCatChem* **2018**, *10*, 4980–4986.
[22] S. Luo, Y. Zhao, K. Pan, Y. Zhou, G. Quan, X. Wen, X Pan, C. Wu, *Biomater. Sci.* **2021**, *9*, 6772–6786.

ChemistryOpen

Research Article
doi.org/10.1002/open.202100288

Chemistry Europe
European Chemical
Societies Publishing

[23] Z. Huang, Z. Yang, M. Z. Hussain, Q. Jia, Y. Zhu, Y. Xia, *J. Mater. Sci. Technol.* **2021**, *84*, 76–85.

[24] F. Subhan, S. Aslam, Z. Yan, M. Yaseen, A. Zada, M. Ikram, *Sep. Purif. Technol.* **2021**, *265*, 118532–118542.

[25] a) S. Guan, R. Yu, F. Guo, Y. Fang, L. Ji, *Ionics* **2021**, *27*, 1633–1643; b) X. Zhong, L. Wang, Z. Z. Zhuang, X. L. Chen, J. Zheng, Y. L. Zhou, G. L. Zhuang, X. N. Li, J. G. Wang, *Adv. Mater. Interfaces* **2017**, *4*, 1601029–1601038.

[26] K. Lee, R. Hahn, M. Altomare, E. Selli, P. Schmuki, *Adv. Mater.* **2013**, *25*, 6133–6137.

[27] M. Zhang, S. Zou, S. Mo, J. Zhong, D. Chen, Q. Ren, M. Fu, P. Chen, D. Ye, *Chemosphere* **2021**, *262*, 127738–127748.

[28] L. Belles, C Moularas, S. Smykała, Y. Deligiannakis, *Nanomaterials* **2021**, *11*, 925–942.

[29] M. Schmal, R. Scheunemann, N. F. P. Ribeiro, J. F. Bengoa, S. G. Marchetti, *Appl. Catal. A* **2011**, *392*, 1–10.

[30] a) T. Jermwongratanachai, G. Jacobs, W. Ma, W. D. Shafer, M. Kumaran, P. Gao, B. Kitiyanan, B. H. Davis, J. L. S. Klettlinger, C. H. Yen, D. C. Cronauer, A. J. Kropf, C. L. Marshall, *Appl. Catal. A* **2013**, *464–465*, 165–180; b) C. Navas-cárdenas, N. Benito, E. E. Wolf, F. Gracia, *Appl. Catal. A* **2019**, *576*, 11–19.

[31] L. Liu, X. Tai, X. Zhou, C. Xin, Y. Yan, *Sci. Rep.* **2017**, *7*, 12709–12717.

[32] a) L. Li, S. Liu, R. Jiang, Y. Ji, H. Li, X. Guo, L. Jia, Z. Zhong, F. Su, *ChemCatChem* **2021**, *13*, 1568–1577; b) R. Yadav, V. Verma, A. Mishra, N. Pal, A. Khan, A. K. Sinha, *J. CO₂ Util.* **2021**, *47*, 101502–101512.

[33] a) L. Liu, X. Tai, X. Zhou, J. Hou, Z. Zhang, *J. Alloys Compd.* **2019**, *790*, 326–336; b) L. L. Liu, X. J. Zhou, Y. M. Yan, J. Zhou, W. P. Zhang, X. S. Tai, *Polymer* **2018**, *10*, 1089–1114; c) A. K. Singh, Q. Xu, *ChemCatChem* **2013**, *5*, 3000–3004; d) Q. Q. Guan, B. Wang, X. S. Chai, J. Liu, J. J. Gu, P. Ning, *Fuel* **2017**, *205*, 130–141; e) R. Kardanpour, S. Tangestaninejad, V. Mirkhani, M. Moghadam, I. Mohammadpoor-Baltork, A. R. Khosropour, F. Zadehahmadi, *J. Organomet. Chem.* **2014**, *761*, 127–133.

[34] L. Liu, X. Zhou, L. Guo, S. Yan, Y. Li, S. Jiang, X. Tai, *RSC Adv.* **2020**, *10*, 33417–33427.

[35] a) A. Sárkány, *React. Kinet. Catal. Lett.* **1999**, *68*, 153–163; b) A. Sarkany, *Appl. Catal. A* **1997**, *165*, 87–101.

[36] a) X. Zhang, Y. C. Guo, Z. C. Zhang, J. S. Gao, C. M. Xu, *J. Catal.* **2012**, *292*, 213–226; b) A. Hugon, L. Delannoy, C. Louis, *Gold Bull.* **2009**, *42*, 310–320.

[37] C. Q. Hu, J. H. Sun, D. J. Kang, Q. S. Zhu, Y. F. Yang, *Catal. Sci. Technologies* **2017**, *7*, 2717–2728.

[38] C. Yoon, M. X. Yang, G. A. Somorjai, *Catal. Lett.* **1997**, *46*, 37–41.